Composite Structures 300 (2022) 116106

Contents lists available at ScienceDirect

Composite Structures

journal homepage: www.elsevier.com/locate/compstruct

Time-dependent behavior of NSM CFRP-strengthened RC beams under different service temperatures

Younes Jahani, Marta Baena *, Alba Codina, Cristina Barris, Lluís Torres

AMADE, Polytechnic School, University of Girona, 17003 Girona, Spain

ARTICLE INFO

Keywords:
NSM FRP-strengthening
Long-term load
Service temperature
Time-dependent deflections

ABSTRACT

The use of fiber reinforced polymer (FRP) for flexural strengthening of reinforced concrete (RC) beams has become a popular strengthening technique. Significant amount of work is available on the short-term flexural behavior of RC beams strengthened with near-surface mounted (NSM) technique. However, their time-dependent flexural behavior, specifically under high service temperature, has not yet been addressed. This paper presents an experimental work to evaluate the time-dependent behavior of NSM carbon FRP (CFRP)-strengthened RC beams. The experimental program included 23 beams, where the effect of different parameters such as strengthening (CFRP) area, steel reinforcement ratio and applied temperature (20 and 50 °C) have been considered. Experimental results show that the effect of strengthening area is significant on the flexural short-term response of the beams, while minor effects are found on the time-dependent deflections. On the other hand, increasing the service temperature has no significant effect on the short-term tests, but it produces a large increase in the time-dependent deflection of the specimens. Finally, an analytical procedure for the prediction of time-dependent deflections, which is based on the age-adjusted effective modulus method (AEMM), is presented. Good agreement between the experimental results and analytical predictions on time-dependent deflections is shown.

1. Introduction

Strengthening of reinforced concrete (RC) structures may become necessary due to different reasons such as increase in the service loads, design code changes, earthquake activities, deficiencies resulting from environmental effects (e.g. corrosion), changes in the occupancy of buildings, etc. [1,2]. In the last decades, fiber reinforced polymer (FRP) materials have been accepted to be used in two of the principal strengthening techniques for RC elements, namely externally bonding reinforcement (EBR) and near-surface mounted (NSM) systems. In the EBR reinforcing technique, the FRP sheets or laminates are bonded to the tensile concrete surface of the damaged member. In the NSM technique, grooves are cut in the tensile face of the RC element where the FRP strips/bars are inserted and bonded. Therefore, due to the confinement provided by surrounding concrete and epoxy, NSM FRP-strengthening technique is less exposed to aggressive environment (and other detrimental effects) and less prone to premature debonding [3–6].

RC elements are usually subjected to long-term loads that can affect their structural performance in terms of time-dependent deflections, loading capacity and failure mode [7–10]. Time-dependent deflections are a function of the loading history (and its effect on concrete mechanical properties), age of concrete at the time of loading, the magnitude and duration of the long-term load and material properties. Within material properties, creep and shrinkage of concrete, which are dependent on environmental conditions, are of main importance [11].

Significant amount of work has been done to study the time-dependent behavior of EBR FRP-strengthened RC elements [9,12–17], where different amounts of carbon FRP (CFRP) area and long-term load levels were considered. The results showed that larger time-dependent deflections were obtained when higher levels of long-term load were applied. Besides, the contribution of CFRP strengthening systems to RC elements under flexural long-term loading was not significant when compared to elements under flexural instantaneous loading [9,13].

Unlike the EBR FRP-strengthened system, few works exist in the literature regarding the time-dependent behavior of NSM FRP-strengthened RC beams [18–21]. Sena-Cruz et al. [18], experimentally studied the time-dependent behavior of slab specimens strengthened with NSM CFRP strips. The load was applied in two steps, first 40 % of long-term load was applied for a duration of 78 days, later the load

* Corresponding author.
E-mail address: marta.baena@udg.edu (M. Baena).

https://doi.org/10.1016/j.compstruct.2022.116106
Received 9 May 2022; Received in revised form 28 July 2022; Accepted 11 August 2022
Available online 26 August 2022

increased to 100 % for a duration of 55 days. The results showed that the majority of time-dependent deflection occurred at the first step of the loading. Moawad et al. [19] experimentally studied the time –dependent behavior of different series of NSM CFRP-strengthened RC beams with different loading histories and sectional properties. Results showed the influence of the loading sequences and levels of loading in combination with the other parameters. The specimens with higher concrete strength resulted in a larger ratio of time-dependent deflections to instantaneous deflection. Moreover, for the strengthened specimens with compression steel reinforcement, the effectiveness of NSM strengthening was more pronounced in reducing the deflections. Finally, the effect of the long-term load on the residual flexural capacity of NSM CFRP-strengthened RC beams was experimentally studied [20] and an analytical work to predict the time-dependent response of the specimens was presented [21]. With increase in the long-term load, the residual capacity of beams decreased. Furthermore, all specimens failed by end-debonding, but for higher long-term load, the end-debonding occurred in longer bonded length with larger bond deterioration. In addition, the same trend in time-dependent strain evolution in FRP was observed from both experimental data and analytical procedures.

The structures under long-term loading are usually exposed to temperature variation during the different seasons of the year. Being epoxy adhesives the most common ones used in NSM strengthening, and due to their nature, special attention should be given to high service temperature (near or beyond the glass transition temperature, T_g, of the epoxy adhesive) [22–25]. In this sense, the instantaneous behavior of NSM FRP-strengthened RC beams under room temperature [26–34] and elevated temperature (fire conditions) [35–39] has received considerable attention, but less work has been done on the effect of high service temperature [40–43].

According to the literature, few works have been performed to study the time-dependent behavior of NSM FRP-strengthened RC members, and, to the best of authors knowledge, none of them account for the effect of high service temperature on the time-dependent deflections and structural performance. Therefore, the purpose of the present study is to investigate the time-dependent behavior of NSM CFRP-strengthened RC beams subjected to room temperature (20 °C) and high service temperature (50 °C). To this end, a total of 23 beams were cast, where the effect of different parameters was considered (i.e. level of strengthening (CFRP area), steel reinforcement ratio and applied temperature (20 and 50 °C)). Experimental results are presented and discussed in terms of instantaneous load–deflection curves, time-dependent and total deflections, time-dependent strain in concrete, failure modes, residual flexural strength of tested specimens and aging effect. Furthermore, an analytical procedure to predict the time-dependent deflection in NSM CFRP-strengthened RC beams is presented. The analytical procedure is based on the age-adjusted effective modulus method (AEMM) [11,44].

2. Experimental program

2.1. Test matrix and test setup

The experimental program included 23 RC beams distributed in three series as follows (see Table 1): 10 beams were tested under short-term load and were considered as reference specimens (Series 1), 10 beams were tested under long-term load to examine their time-dependent behavior (Series 2) and, finally, 3 beams were cast and rested in the lab (without any loading) to be tested at the end of the long-term experimental program. Series 1 and Series 2 were divided into two groups to evaluate the effect of steel reinforcement ratio ($\rho = 0.79$ % and 1.14 % for Group 1 and 2, respectively). Group 1 included two control beams and four NSM CFRP-strengthened RC beams, with two different amounts of CFRP strengthening, subjected to 20 and 50 °C. In Group 2, two control beams and two NSM CFRP-strengthened RC beams, strengthened with three CFRP strips, were subjected to 20 and 50 °C.

Specimens' designation reads X-Y-Z-T, where X indicates the type of loading (ST standing for short-term load, LT standing for long-term load and AG meaning aging effect). Moreover, Y denotes the type of beam (CB meaning control beam, and SB1S and SB3S referring to strengthened beams with one and three CFRP strips, respectively). Furthermore, Z indicates the Group that specimen belongs to (i.e. thus indicating the steel reinforcement ratio). Finally, T stands for the testing temperature. For instance, ST-CB-1–20, refers to the control beam in Group 1 ($\rho =$ 0.79 %) tested under short-term loading at 20 °C. Furthermore, LT-SB3S-2–50 refers to a beam strengthened with three CFRP strips from Group 2 ($\rho = 1.14$ %) and tested under long-term loading at 50 °C.

The beams were tested under a four-point bending configuration (see Fig. 1). The sectional dimensions of the beams were 180 × 140 mm and the total and clear length of specimens were 2400 mm and 2200 mm, respectively. Specimens in Group 1 were reinforced with two steel rebars with a diameter of 10 mm and two steel rebars with a diameter of 6 mm in the tension and compression side of the beam, respectively ($\rho =$ 0.79 %). In Group 2, rebars with a diameter of 12 mm and 8 mm were used in tension and compression side of the beam, respectively ($\rho = 1.14$

Table 1
Text matrix.

Series	Loading type	Group	Steel reinforcement ratio, ρ (%)	Beam ID	Testing Temperature (°C)	No. of CFRP strips	Total CFRP area (mm^2)
Series 1	Short-term	Group 1	0.79	ST-CB-1–20	20	–	–
				ST-CB-1–50	50	–	–
				ST-SB1S-1–20	20	1	14
				ST-SB1S-1–50	50	1	14
				ST-SB3S-1–20	20	3	42
				ST-SB3S-1–50	50	3	42
		Group 2	1.14	ST-CB-2–20	20	–	–
				ST-CB-2–50	50	–	–
				ST-SB3S-2–20	20	3	42
				ST-SB3S-2–50	50	3	42
Series 2	Long-term	Group 1	0.79	LT-CB-1–20	20	–	–
				LT-CB-1–50	50	–	–
				LT-SB1S-1–20	20	1	14
				LT-SB1S-1–50	50	1	14
				LT-SB3S-1–20	20	3	42
				LT-SB3S-1–50	50	3	42
		Group 2	1.14	LT-CB-2–20	20	–	–
				LT-CB-2–50	50	–	–
				LT-SB3S-2–20	20	3	42
				LT-SB3S-2–50	50	3	42
Series 3	Aging	Group 1	0.79	AG-CB-1–20	20	–	–
				AG-SB1S −1–20	20	1	14
				AG-SB3S-1–20	20	3	42

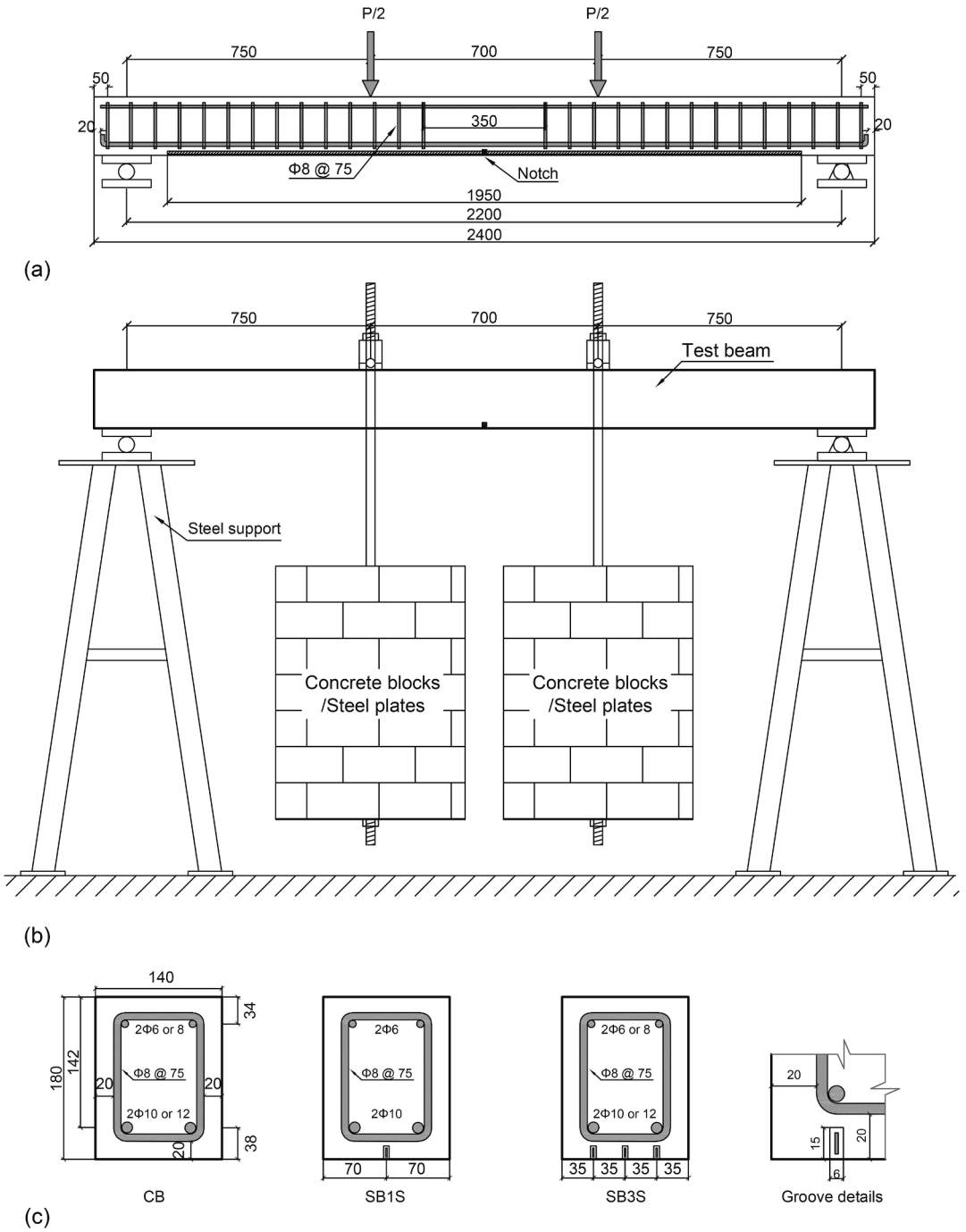

Fig. 1. Details of the tested beams: (a) Short-term setup; (b) Long-term setup and (c) Beam sections (dimensions in mm).

%). To avoid shear failure, stirrups with a diameter of 8 mm were placed every 75 mm in all beams. Furthermore, to strengthen the beams in flexure, and following *fib* Bulletin 90 [45] recommendations, grooves with dimensions of 6 × 15 mm were cut in the soffit of the beams, and strips with dimensions of 1.4 × 10 mm were introduced using an epoxy adhesive. Moreover, a 5 × 15 mm notch was created in the midspan of all beams to act as a crack initiator. For Series 1 and 3 (short-term load before and after aging), the flexural test was performed under displacement control at a rate of 0.6 mm/min, whereas for Series 2 (long-term load), concrete blocks and steel plates were used as dead-weight (see Fig. 1b).

2.2. Instrumentation

Beam instrumentation is shown in Fig. 2. A set of linear vertical displacement transducers (LVDTs) were placed in the beam to register the movement of the beam. One LVDT was used in the midspan of the beam to measure the central deflection (LVDT1). In Series 1 and 3 (subjected to short-term loading), two LVDTs (LVDT 2 and 3) were placed at supports sections to measure the supports settlement. In addition to LVDTs, one strain gauge was installed in the midspan of the specimens to register the strain at the top fiber of concrete (SG_C).

In those specimens subjected to the temperature, heating blankets (installed to the soffit of the beam) were used to heat up the beams up to the target temperature (i.e. 50 °C). The heating process was controlled by proportional integral derivative (PID) controller, and Type-T

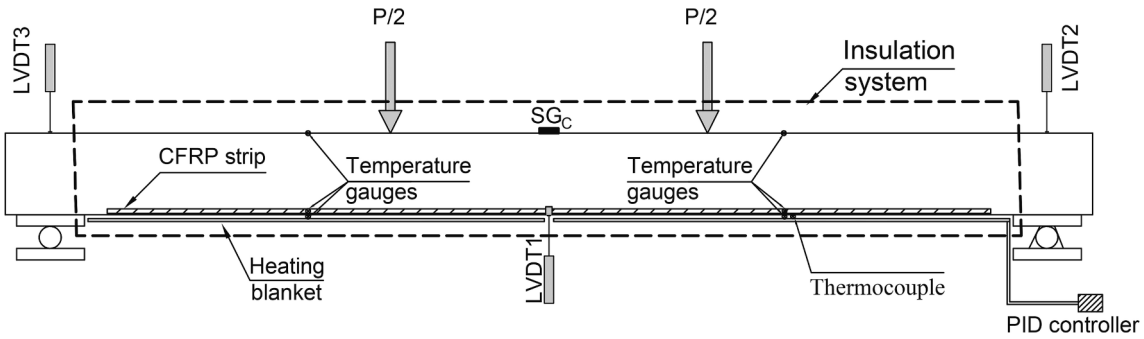

Fig. 2. Beams instrumentation: Position of the linear vertical displacement transducers (LVDTs), concrete strain gauges, temperature gauges, heating system and insulation system.

thermocouples, installed between the heating blanket and the soffit of the beam, were used as temperature controller sensor. In order to ensure a better heat distribution along the beam, an isolation system was used. To monitor and record the temperature during the heating process and flexural testing, different temperature gauges were installed on concrete surface at the top and bottom of the beam, on the surface of the CFRP (it was installed before introducing FRP into the grooves) and on the surface of epoxy adhesive (see Fig. 2). The beams were left to be heated-up for 24 h prior to testing (in both short-term and long-term load) until the average temperature in the soffit of the beam was stabilized to the target value. A general view of short-term and long-term load setup is shown in Fig. 3.

2.3. Temperature and humidity

Registration of lab conditions (temperature and humidity) started the day of concrete casting and continued till the end of the experimental program. An average temperature and humidity of 19.6 °C and 64 % were registered, respectively (see Fig. 4a). In addition, the evolution of temperature and humidity of beams under 50 °C was registered during the heating (24 h prior to testing) until the end of the long-term loading. Average values for temperature and humidity read 50.4 °C and 16 %, respectively (see Fig. 4b).

2.4. Materials

2.4.1. Concrete

The specimens were cast in the structural lab with ready-mix concrete. The cement type was I-42.5R, with a content of 390 kg/m^3. The maximum aggregate size was 12 mm, and the water/cement ratio was 0.41. A viscosity modifier and underwater admixture were used to improve workability. In order to determine the mechanical properties of concrete, cylinder specimens with 300 mm nominal height and 150 mm nominal diameter were used. The compressive strength (f_c), tensile strength (f_t) and modulus of elasticity (E_c) of the concrete were determined according to UNE-EN 12390–3 [46], UNE-EN 12390–6 [47], and ASTM C469 [48] standards, respectively. The mechanical properties of concrete at different ages is summarized in Table 2.

The time-dependent behavior of the concrete was determined according to ASTM C512-02 [49]. To this end, four cylindrical specimens (150 mm diameter and 450 mm height) with an embedded strain gauge were manufactured. Two of the four cylinders were kept at 20 °C and the other two were heated up to 50 °C. Each pair of concrete cylinders was stacked on a loading frame and loaded with a long-term load level of 0.35f_c (the same long-term load level in all specimens). The long-term load was applied at the same time as the beams.

To measure free shrinkage strain in concrete (ε_{sh}), two concrete prisms, having the same concrete beam section (180 × 140 mm) and 1 m length, were instrumented with an embedded strain gauge and left unloaded at the same temperature and humidity as beam specimens. The strain evolution with time for both shrinkage specimens (at 20 °C and 50 °C) is shown in Fig. 5a. For the specimen submitted to 50 °C, heating started at the same time as heating of the long-term specimens (Series 2). The effect of heating on concrete shrinkage is clearly visible. In the shrinkage specimen subjected to 50 °C, the thermal strain was also considered in the strain registration. Registers of maximum shrinkage at the end of long-term loading are summarized in Table 3, with shrinkage corresponding to the heated specimen being 35 % higher than that of the specimen at lab conditions.

The concrete creep coefficient was obtained according to Eq. (1):

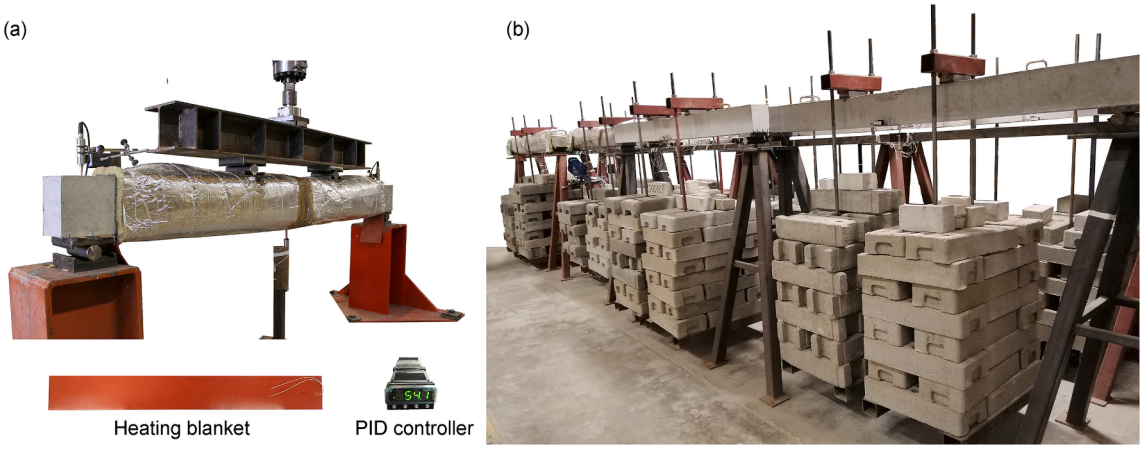

Fig. 3. General view of experimental setup and heating system: (a) Short-term load setup and (b) Long-term load setup.

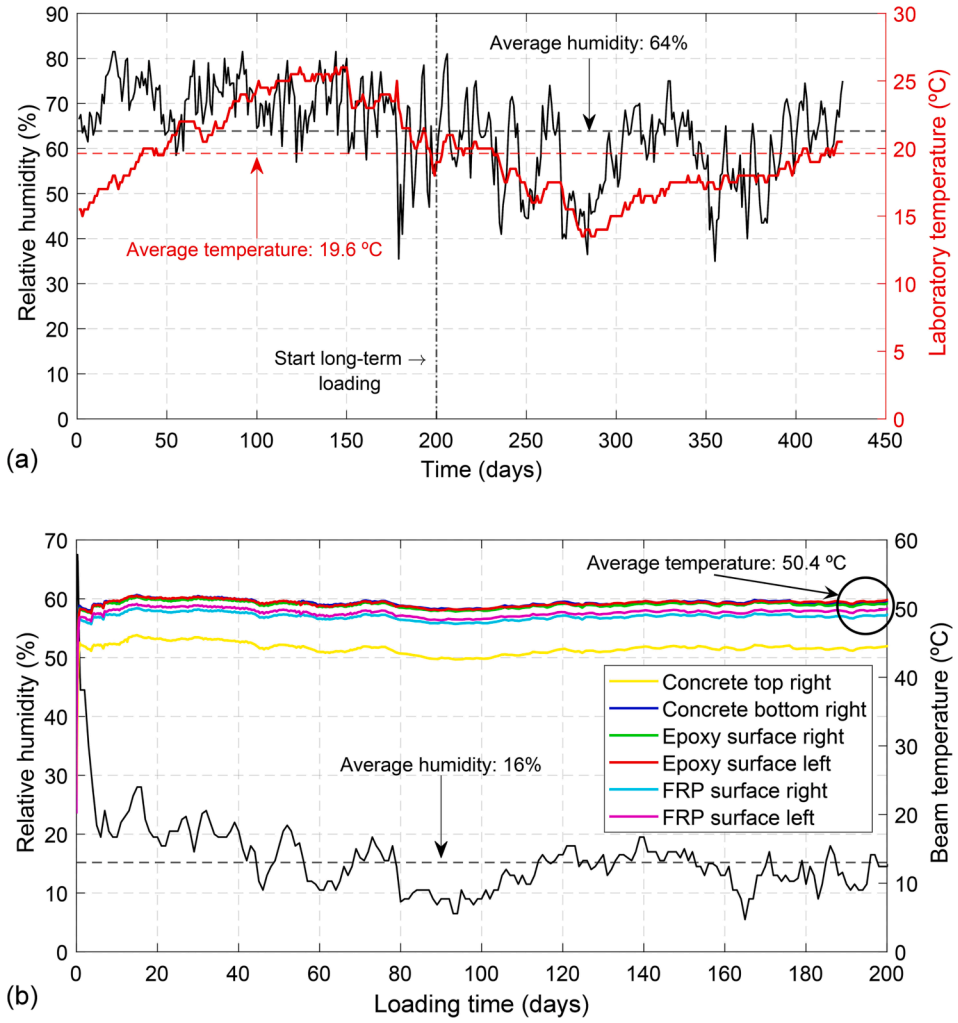

Fig. 4. Registers on temperature and humidity: (a) Lab condition and (b) Inside the beam at 50 °C.

Table 2
Concrete mechanical properties.

Concrete age (days)	Compressive strength, f_c (MPa)	Tensile strength, f_t (MPa)	Modulus of elasticity, E_c (GPa)
90[a]	48.1 (2.3 %)[d]	3.7 (6.0 %)[d]	41.2 (5.3 %)[d]
200[b]	48.3 (2.2 %)[d]	3.7 (9.0 %)[d]	41.9 (4.5 %)[d]
430[c]	53.7 (0.8 %)[d]	3.6 (9.4 %)[d]	47.6 (1.9 %)[d]

[a] Age at short-term test of Series 1.
[b] Age at long-term test of Series 2.
[c] Age at residual flexural test of Series 2 and short-term test of Series 3.
[d] Coefficient of variation (CoV) indicated in brackets.

$$\varphi_c(t,t_0) = \frac{\varepsilon_c(t,t_0) - \varepsilon_{cs}(t,t_0) - \varepsilon_{ci}(t_0)}{\varepsilon_{ci}(t_0)} \quad (1)$$

where t is the loading time, t_0 is the concrete age at the start of loading, $\varphi_c(t,t_0)$ is the concrete creep coefficient, $\varepsilon_c(t,t_0)$ is the total concrete strain, $\varepsilon_{cs}(t,t_0)$ is the concrete shrinkage strain and $\varepsilon_{ci}(t_0)$ is the instantaneous concrete strain caused by the long-term load.

Due to technical issues in the setup of the concrete creep specimen subjected to 50 °C, the concrete creep coefficient was experimentally determined only for specimens at 20 °C (see Fig. 5b). Existing formulation from Model Code 2010 [11] was used to estimate the concrete creep coefficient for the concrete at 50 °C. Experimental values and analytical prediction of concrete creep coefficient are presented in Table 3. For comparison purposes, analytical prediction on concrete creep coefficient of specimen subjected to 20 °C is also included.

2.4.2. Steel reinforcement

Mechanical properties of steel bars were obtained from tension tests based on UNE-EN ISO 15630–1 [50]. The yielding strength (f_y), the ultimate strength (f_u) and the modulus of elasticity (E_s) were 586.4 MPa (CoV = 2.3 %), 707.7 MPa (CoV = 1.7 %) and 205.1 GPa (CoV = 1.0 %) respectively.

2.4.3. CFRP strips

CFRP strips, consisting of unidirectional carbon fibers (with a volume content fiber higher than 68 %) held together by an epoxy vinyl ester resin matrix, were used for strengthening the specimens [51]. The mechanical properties of the CFRP strips were obtained according to ISO 527–5 [52] recommendations. An ultimate tensile strength ($f_{u,FRP}$) of 2251.4 MPa (CoV = 3.2 %), an ultimate tensile strain ($\varepsilon_{u,FRP}$) of 0.0133 (CoV = 7.2 %), and a modulus of elasticity (E_{FRP}) of 169.5 GPa (CoV = 6.3 %) were obtained [40].

2.4.4. Epoxy adhesive

The adhesive used in this study is a high performance, solvent-free, thixotropic, and grey two-component epoxy adhesive specially developed for bonding CFRP to concrete under the commercial name of S&P220HP. According to the manufacturer's product data sheet [53], the components A (resin) and B (hardener) should be mixed at a ratio of 2:1 by weight, and the suggested curing duration is 7 days. Tensile

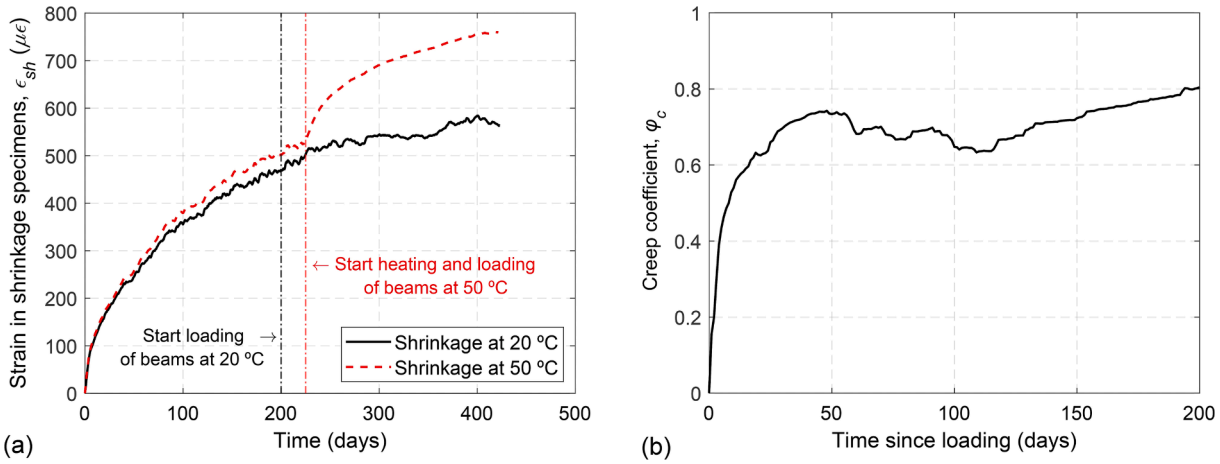

Fig. 5. Experimental time-dependent behavior of concrete: (a) Strain in shrinkage specimens at 20 and 50 °C and (b) Creep coefficient at 20 °C.

Table 3
Concrete creep coefficient and shrinkage strain.

Temperature (°C)	Concrete creep coefficient, φ_c		Experimental shrinkage strain, ε_{sh} ($\mu\varepsilon$)
	Experimental	Model Code 2010 [11]	
20	0.80	0.60	563
50	-[1]	2.64	759

[1] Not available due to failure in setup.

properties of the epoxy adhesive were determined by iSO-527–1 [54] specifications (see Table 4) [24]. To evaluate the effect of temperature on mechanical properties of the epoxy, the specimens were tested under 20 °C and 50 °C. The tensile strength ($f_{u,epoxy}$) and modulus of elasticity (E_{epoxy}) at 50 °C decreased by 30 % and 47 %, respectively, when testing temperature changed from 20 °C to 50 °C. Moreover, the glass transition temperature (T_g) of epoxy was also determined with differential scanning calorimetry (DSC) [55] and dynamic mechanical analysis (DMA) [56]. According to test results, the T_g of epoxy was in the range of 53.9–65.3 °C [40].

The creep coefficient of epoxy adhesive (φ_{epoxy}) was also evaluated at 20 and 50 °C (see Fig. 6). Three levels of long-term load (causing 20 %, 40 % and 60 % of epoxy ultimate strain, 0.0035, obtained from tensile test) were applied to the specimens for a duration of 40 days (1000 h), which is similar to the duration used in the literature [22,57–59]. The long-term loading was applied through a gravity loading system with a lever arm with a magnification factor of 4 [22,60]. The temperature and humidity conditions applied during the epoxy tensile creep tests were the same as those of the beams. For each temperature, two specimens were tested, and all specimens included two strain gauges (one at each side). The creep coefficient of epoxy adhesive was obtained according to Eq. (2):

$$\varphi_{epoxy}(t,t_0) = \frac{\varepsilon_e(t,t_0) - \varepsilon_e(t_0)}{\varepsilon_e(t_0)} \quad (2)$$

where ε_e (t,t_0) is the epoxy adhesive strain with time and ε_e (t_0) is the epoxy adhesive strain at the loading moment.

According to experimental results, epoxy creep coefficient at 20 °C was affected by the sudden drop in humidity and temperature in the lab taking place around 200 h after loading (see Fig. 6a). Besides, specimens tested at 50 °C failed after a few hours of loading (see Fig. 6b).

2.5. Test procedure

In this experimental program, 4 loading stages were considered. In stage 1, the beams of Series 1 were tested under four-point bending configuration (see Fig. 1a) to obtain their short-term flexural response. Tests were performed under displacement control mode at a rate of 0.6 mm/min.

In stage 2, prior to long-term test, beams were subjected to pre-loading in order to ensure a level of cracking corresponding to the service load. To this end, beams in Series 2 were subjected to two loading/unloading cycles up to service load level, P_{ser}. The service load was calculated by limiting the stress in compressed concrete ($\sigma_c < 0.6f_c$) and steel reinforcement ($\sigma_s < 0.8f_y$) [61]. For this pre-loading stage, the same test setup and loading rate as in stage 1 was used.

In stage 3, after the pre-loading, specimens in Series 2 were moved to the long term loading frames (Fig. 1b) and the long-term load was applied for a duration of 200 days. The long-term load was chosen to obtain a concrete compressive stress of 0.35 f_c, so that linear creep behavior of concrete was ensured by being under the Model Code 2010 limitation [11].

Finally, in stage 4, and after the long-term test, specimens in Series 2 were tested up to failure to evaluate their residual flexural strength. Additionally, specimens of Series 3, that were resting in the lab for aging, were tested to obtain their short-term flexural response. In this stage, the same test setup and loading rate as in stages 1 and 2 was used.

3. Experimental results and discussions

3.1. Short-term tests results

Results of short-term flexural tests (Series 1) are presented in Fig. 7 in terms of load versus midspan deflection curves. In each curve, three phases can be distinguished: i) an initial linear behavior representing the elastic behavior of the uncracked element; ii) a second phase, starting at

Table 4
Mechanical properties of epoxy adhesive [24].

Testing temperature (°C)	Tensile strength, $f_{u,epoxy}$ (MPa)	$f_{u,epoxy\text{-}50}$ / $f_{u,epoxy\text{-}20}$	Modulus of elasticity, E_{epoxy} (MPa)	$E_{epoxy\text{-}50}$ / $E_{epoxy\text{-}20}$
20	28.0 (0.4 %)[a]	–	8102.4 (0.8 %)[a]	–
50	19.6 (3.6 %)[a]	0.7	4289.6 (2.3 %)[a]	0.53

[a] Coefficient of variation (CoV) indicated in brackets.

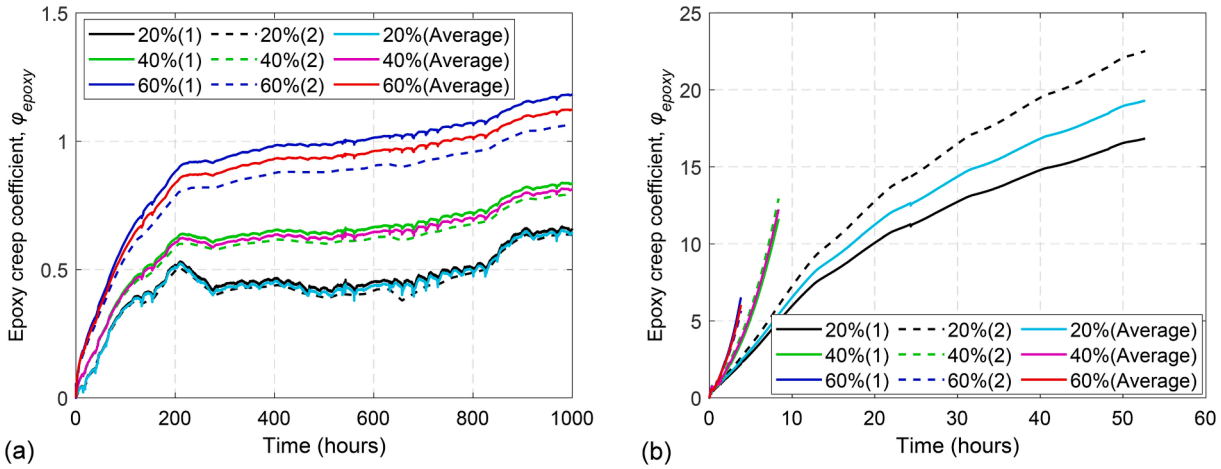

Fig. 6. Creep coefficient of epoxy adhesive (a) at 20 °C and (b) at 50 °C.

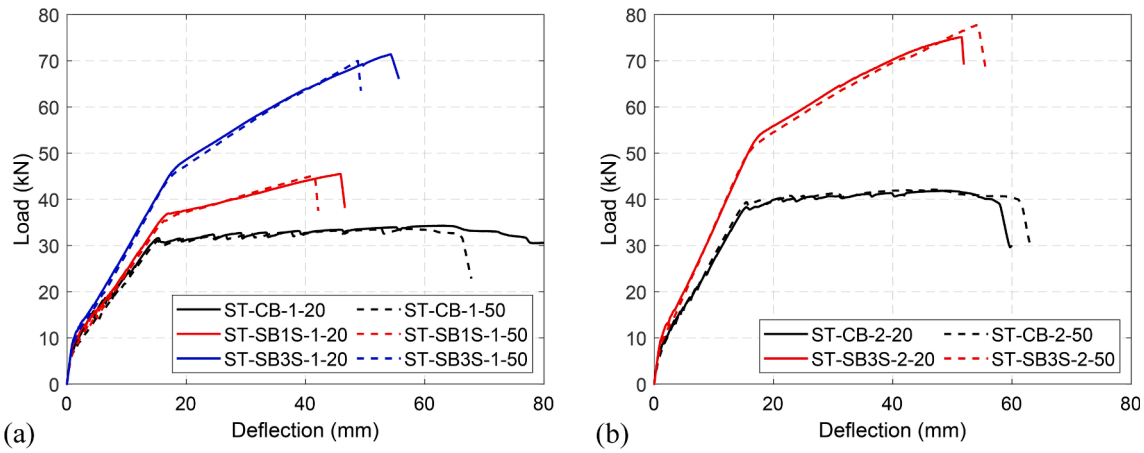

Fig. 7. Load-deflection curves of specimens in Series 1: (a) Group 1 (ρ = 0.79 %) and (b) Group 2 (ρ = 1.14 %).

the cracking load (P_{cr}), where stiffness decreases and load can be increased up to yielding of steel reinforcement; and iii) a post-yielding phase up to failure. For the case of unstrengthened beams (CB), no significant differences between yielding load (P_y) and ultimate load (P_u) exist. For the case of strengthened beams, load can be further increased after steel yielding until the ultimate load. Experimental results of short-term tests (Series 1) are presented in Table 5. As a general result, the increase in the CFRP strengthening area produces an increase in stiffness in the post-cracking and post-yielding stages, which results in larger yielding loads, P_y, and ultimate loads, P_u. According to results presented in Table 5, larger benefits of the CFRP strengthening system were obtained in beams with lower steel reinforcement ratio, as expected and depicted by the comparison between the strength increase ratios of specimens in Groups 1 and 2. Finally, no significant effect of temperature is visible in the load–deflection curves. The similarity in short-term responses between specimens tested at 20 °C and 50 °C can be attributed to the fact that 50 °C was below the T_g of the epoxy (53.9 °C < T_g < 65.3 °C) and epoxy adhesive was post-cured and therefore its mechanical properties improved [24,25,40].

Table 5
Experimental results of specimens in Series 1 under short-term load.

Specimen ID	P_{cr} (kN)	P_y (kN)	P_u (kN)	Strength increase ratio [a]	Failure mode [b]
ST-CB-1–20	7.43	30.75	34.28	–	CC
ST-CB-1–50	7.00	30.00	33.57	–	CC
ST-SB1S-1–20	7.82	36.88	45.50	1.33	FR
ST-SB1S-1–50	6.00	35.36	45.15	1.34	FR
ST-SB3S-1–20	8.85	46.50	71.40	2.08	FR
ST-SB3S-1–50	6.75	45.25	70.00	2.09	FR
ST-CB-2–20	6.70	37.89	41.84	–	CC
ST-CB-2–50	5.95	38.71	42.10	–	CC
ST-SB3S-2–20	9.60	53.36	75.10	1.79	FR
ST-SB3S-2–50	8.20	51.00	77.68	1.85	FR

[a] Ratio of ultimate load of strengthened beam to ultimate load of the control unstrengthened beam of the same group.
[b] CC = concrete crushing after steel yielding; FR = FRP rupture.

Representative images of failure modes are shown in Fig. 8. Unstrengthened control beams, with and without temperature, failed by concrete crushing (CC) after steel reinforcement yielding. Besides, all strengthened beams failed by FRP rupture, irrespective of the applied temperature and the CFRP strengthening area, and no premature bond failure took place. It should be mentioned that results may change if different test configurations and/or larger temperatures were applied [40].

3.2. Pre-loading

Before the application of the long-term load, specimens of Series 2 were subjected to a pre-loading stage, consisting in two cycles of

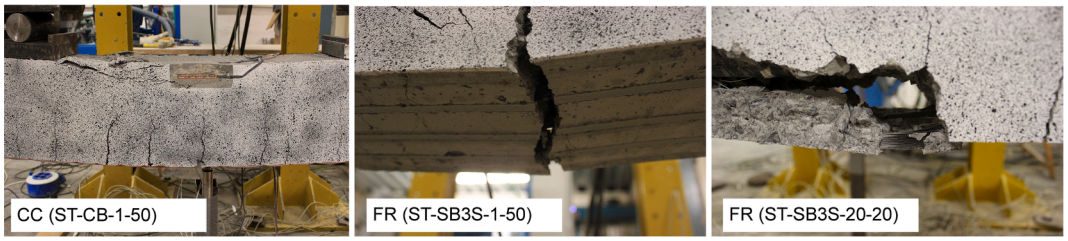

Fig. 8. Representative views of failure modes of specimens in Series 1.

Table 6
Experimental results for pre-loading stage in Series 2.

Specimen ID	P_{ser} (kN)	P_{LT} (kN)	$\delta_{p,0}$ (mm)
LT-CB-1–20	20.4	13.8	2.14
LT-CB-1–50			2.14
LT-SB1S-1–20	24.8		2.21
LT-SB1S-1–50			2.32
LT-SB3S-1–20	27.1		1.93
LT-SB3S-1–50			1.93
LT-CB-2–20	26.5	15.8	2.22
LT-CB-2–50			2.05
LT-SB3S-2–20	30.0		1.86
LT-SB3S-2–50			1.67

loading/unloading. First, the specimens were loaded up to the service load level (P_{ser}); then, two cycles were applied between the minimum load (2 kN) and maximum load (service load). Table 6 shows the experimental data from the pre-loading stage for all of the specimens in Series 2. Finally, the specimens were rested to relax at lab conditions for 1 day prior to the application of the long-term load. Deflections were continuously registered, even during the relaxation period, so that the permanent deflection after a one-day relaxation ($\delta_{p,0}$) could be computed. Fig. 9 presents representative load–deflection curves for the pre-loading process of LT-SB3S-1–20 and LT-SB3S-2–50. In this Figure, P_{LT} stands for level of long-term load to be applied in long-term tests.

3.3. Time-dependent tests results

Following the pre-loading stage, beams in Series 2 were placed according to the setup shown in Fig. 1b to be tested under long-term loading. The vertical transducer at midspan section allowed registering the evolution of deflection due to long-term load. Similarly, the evolution of concrete strains was also recorded.

3.3.1. Deflections

The evolution of the total deflection (δ_{tot}) with time is presented in Fig. 10. The total deflection results from the addition of the permanent deflection after pre-loading stage ($\delta_{p,0}$), the instantaneous deflection after the application of the long-term load (δ_{ins}) and the time-dependent deflection due to long-term load (δ_{td}). The markers in the vertical axis in Fig. 10 represent the permanent deflection after pre-loading stage ($\delta_{p,0}$). Additionally, time-dependent deflections (δ_{td}) are presented in Fig. 11. According to experimental results, summarized in Table 7, the increase of the CFRP strengthening area in specimens tested at 20 °C resulted in a decrease in the three components of the total deflection (i.e. $\delta_{p,0}$, δ_{ins} and δ_{td}), irrespective of the steel reinforcement ratio. This is due to the increase in the tensile reinforcement stiffness and due to the same long-term load being applied in all specimens of the same group (i.e. long-term load to be applied was the same for control specimens and specimens with CFRP strengthening).

Experimental results on specimens tested at 50 °C revealed that the application of a high service temperature (50 °C) did not have remarkable effects on the instantaneous deflection after the application of the long-term load (δ_{ins}), when compared to that of specimens at 20 °C. However, the application of high service temperature had a clear effect on time-dependent deflections (δ_{td}), irrespective of the steel reinforcement ratio. In this sense, in Group 1, the time-dependent deflection in unstrengthened control beam (LT-CB-1–50) increased by 60 % because of the application of 50 °C, and this percentage increase up to 85 % for strengthened beams with either one or three strips (i.e. LT-SB1S-1–50 and LT-SB3S-1–50). Likewise, in Group 2, the time-dependent deflection increased by 86 % and 100 % in unstrengthened control beam (LT-CB-2–50) and strengthened beam (LT-SB3S-2–50), respectively. It should be mentioned that similar time-dependent deflections were obtained within the same Group of specimens tested at 50 °C, so that the time-dependent response of the strengthened beams approached to the unstrengthened beam.

An initial explanation lies in the larger concrete time-dependent

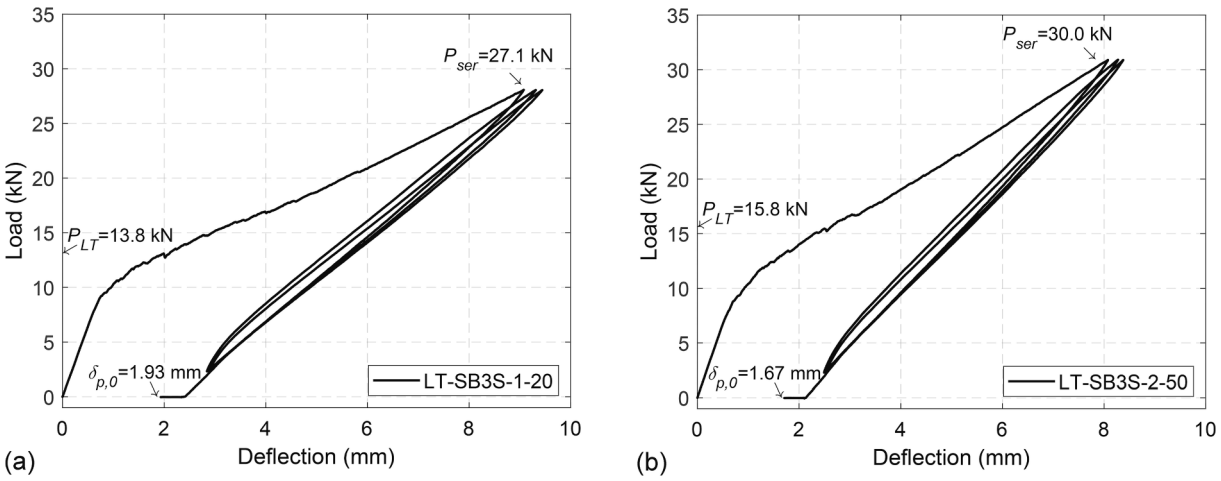

Fig. 9. Representative load–deflection curves for pre-loading process for specimens: (a) LT-SB3S-1–20 and (b) LT-SB3S-2–50.

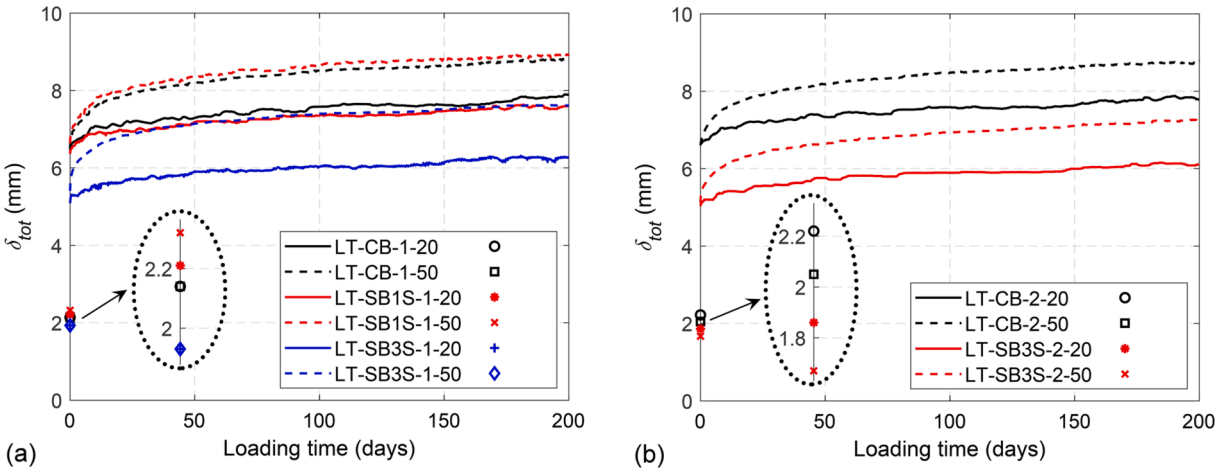

Fig. 10. Total deflection of beams in Series 2: (a) Group 1 (ρ = 0.79 %) and (b) Group 2 (ρ = 1.14 %).

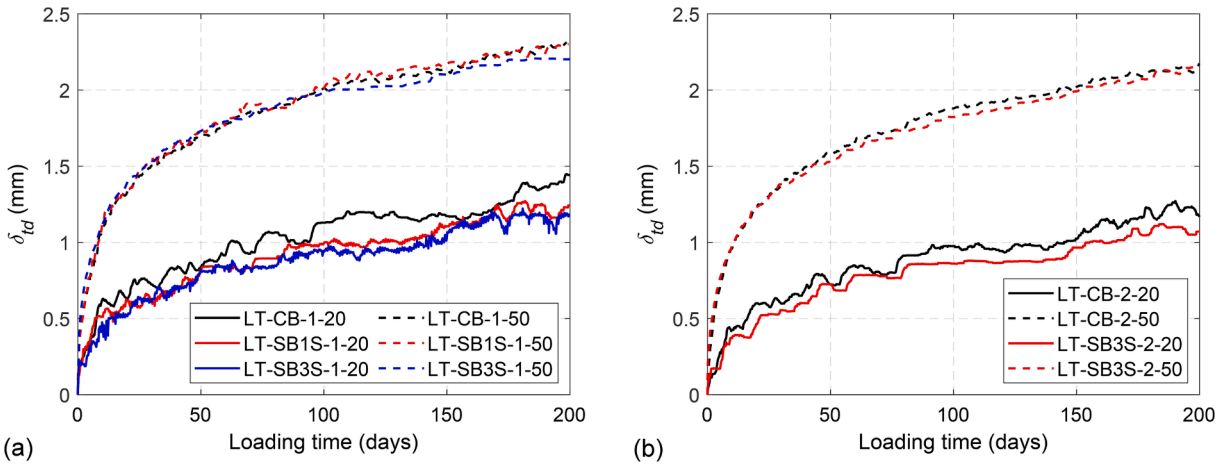

Fig. 11. Time-dependent deflection of beams in Series 2: (a) Group 1 (ρ = 0.79 %) and (b) Group 2 (ρ = 1.14 %).

Table 7
Deflections from long-term load.

Specimen ID	Deflections (mm)				$\delta_{tot}/\delta_{ins,tot}$
	δ_{ins}	$\delta_{ins,tot} = \delta_{ins} + \delta_{p,0}$	$\delta_{td,max}$[a]	$\delta_{tot} = \delta_{ins,tot} + \delta_{td,max}$	
LT-CB-1–20	4.31	6.45	1.44	7.89	1.22
LT-CB-1–50	4.36	6.50	2.31	8.81	1.36
LT-SB1S-1–20	4.15	6.36	1.24	7.6	1.19
LT-SB1S-1–50	4.31	6.63	2.30	8.93	1.35
LT-SB3S-1–20	3.16	5.09	1.18	6.27	1.23
LT-SB3S-1–50	3.48	5.41	2.20	7.61	1.41
LT-CB-2–20	4.39	6.61	1.17	7.78	1.18
LT-CB-2–50	4.55	6.60	2.18	8.78	1.33
LT-SB3S-2–20	3.17	5.03	1.07	6.1	1.21
LT-SB3S-2–50	3.44	5.11	2.14	7.25	1.42

[a] Maximum time-dependent deflection from Fig. 11.

properties (i.e. shrinkage and creep coefficient) at 50 °C. Based on experimental values for concrete shrinkage in prism specimens (see Fig. 5a), the total shrinkage of the specimens from the day of loading increased from 100 με at 20 °C to 240 με at 50 °C. Furthermore, according to analytical predictions presented in Table 3, concrete creep coefficient increased from 0.60 to 2.64, showing a 340 % difference. A secondary cause can be the detrimental effect of temperature on both instantaneous and time-dependent mechanical properties of the epoxy adhesive. In this sense, short-term values of epoxy tensile strength ($f_{u,epoxy}$) and tensile modulus of elasticity (E_{epoxy}) decreased by 30 % and 47 %, respectively, when epoxy was submitted to 50 °C (see Table 4). Additionally, higher creep coefficients were found for epoxy at 50 °C (see Fig. 6). Nevertheless, it should be mentioned that the effect of higher temperature on the time-dependent behavior of concrete seems to be dominant, as the time-dependent deflections of the unstrengthened control beams in Groups 1 and 2 subjected to temperature (i.e. LT-CB-1–50 and LT-CB-2–50) were increased by 60 % and 86 %, respectively.

It should be mentioned that the fluctuations observed in the evolution of deflection at 20 °C (Figs. 10 and 11) were probably due to large humidity variations taking place at the structural lab (see Fig. 4a). For the case of heated specimens (submitted to 50 °C), minimum fluctuations in humidity were observed, because of the good performance of the heating and isolation systems (see Fig. 4b).

The normalized deflections of the specimens (δ_{tot} / $\delta_{ins,tot}$), where $\delta_{ins,tot} = \delta_{ins} + \delta_{p,0}$, are shown in Fig. 12. According to experimental results, larger normalized deflections were obtained in specimens strengthened with three strips, and similar normalized deflections were obtained for beams strengthened with one strip and their counterpart unstrengthened beam. This is due to lower instantaneous deflections ($\delta_{ins,tot}$) for beams with three strips and similar time-dependent deflections (δ_{td}) for

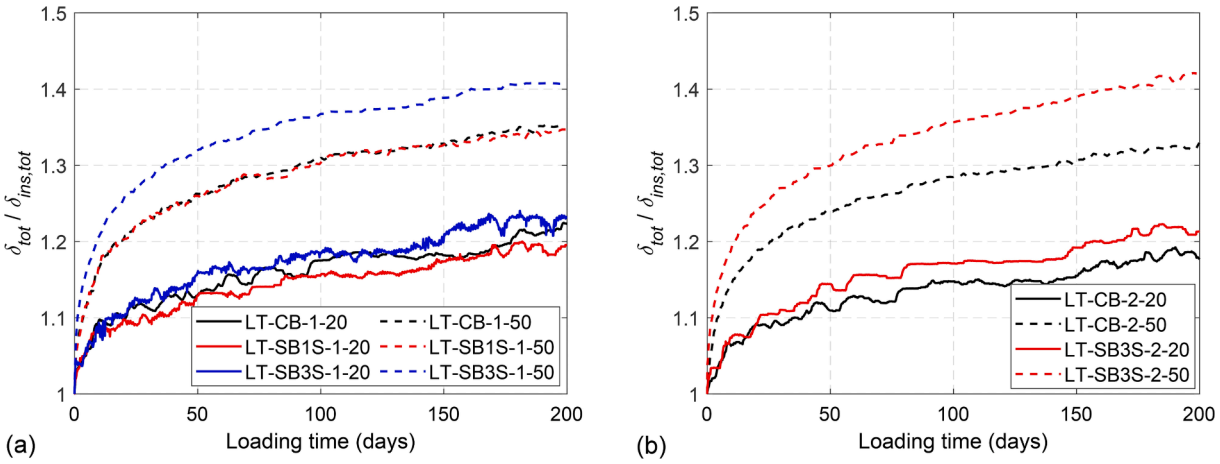

Fig. 12. Ratio of total to instantaneous deflection of beams in Series 2: (a) Group 1 (ρ = 0.79 %) and (b) Group 2 (ρ = 1.14 %).

beams within the same Group. This effect is more clear when deflections of specimens under 50 °C are analyzed.

3.3.2. Concrete strain

The total and time-dependent strain at the top fiber of concrete at the midspan section (see the position of SG_C in Fig. 2) is shown in Figs. 13 and 14 respectively. Similar to evolution of total and time-dependent deflections, strengthening with larger amounts of CFRP area resulted in a reduction in total and time-dependent concrete strain. In addition, the application of high service temperature produced a sharp increase in the time-dependent concrete strain. For instance, for unstrengthened control beams in Group 1 (LT-CB-1–50) and Group 2 (LT-CB-2–50), the time-dependent concrete strain was increased by 65 % and 77 %, respectively. For strengthened beams in Group 1 (LT-SB1S-1–50 and LT-SB3S-1–50) the percentage increased up to 79 % and 88 %, respectively. Furthermore, in strengthened specimens belonging to Group 2 (LT-SB3S-2–50), the time-dependent concrete strain was increased by 136 %. According to the results from unstrengthened beams, and similar to the evolution of time-dependent deflections, time-dependent strains in concrete were mostly affected by concrete time-dependent properties and how they depend on service temperature.

3.4. Residual flexural strength and aging effect

Following long-term tests, specimens in Series 2 were tested up to failure to evaluate their residual flexural strength. The initial deflection prior to the post long-term tests was obtained by registering the ultimate permanent deflection ($\delta_{p,u}$) after removing the long-term load. In addition, specimens in Series 3 were also tested up to failure to evaluate the aging effect on their instantaneous load–deflection response. Fig. 15 shows representative load–deflection curves, and detailed results are listed in Table 8.

The ultimate permanent deflection ($\delta_{p,u}$) was used to plot the load–deflection curves of specimens in Series 2 during their testing up to failure after long-term loading (see Fig. 15). According to the results presented in Table 8, it is worthy to mention that the ultimate permanent deflection of specimens subjected to 50 °C was larger than that of specimens at 20 °C, which was in agreement with the trend in time-dependent deflections.

The comparison between results in Series 1 and Series 2 (black and red lines in Fig. 15, respectively) allows accounting for the residual strength of the beams after long-term load. For the case of unstrengthened control beams, similar yielding loads and post-yielding behavior were obtained. The differences in their ultimate deflection can be attributed to the failure mode (concrete crushing) and the values for concrete compressive strain at failure. For the case of strengthened beams, in general slightly higher values for yielding load and post-yielding stiffness were found for the case of beams submitted to previous long-term load, irrespective of the temperature applied during the long-term tests. It should be mentioned that failure mode for strengthened beams remained to be FRP rupture, except for the case of beams strengthened with three strips in Group 2 (LT-SB3S-2–20 and LT-SB3S-2–50). In these latter cases, premature cracking initiated in the compression zone of the specimens and, due to the increase in deflection

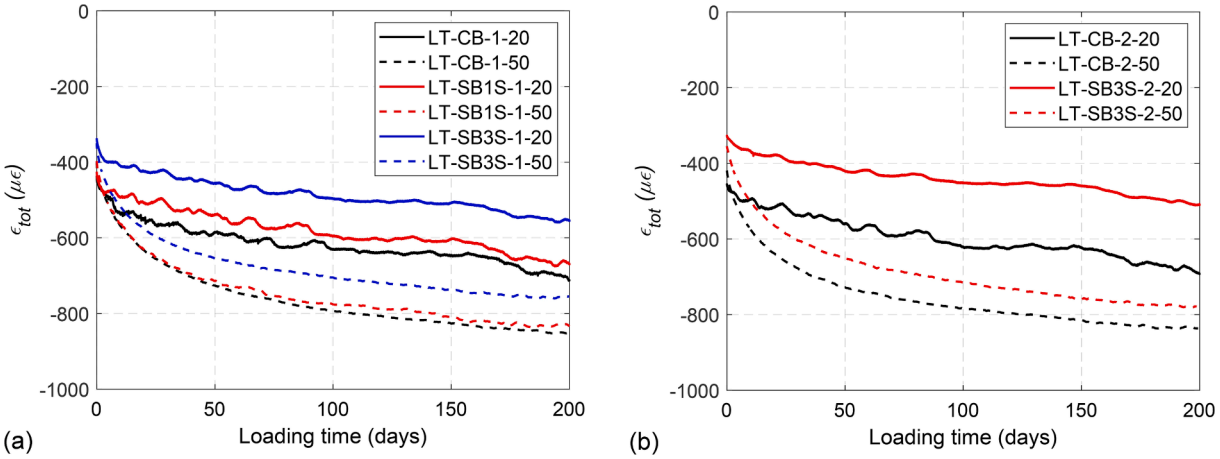

Fig. 13. Top fiber concrete total strain evolution: (a) Group 1 (ρ = 0.79 %) and (b) Group 2 (ρ = 1.14 %).

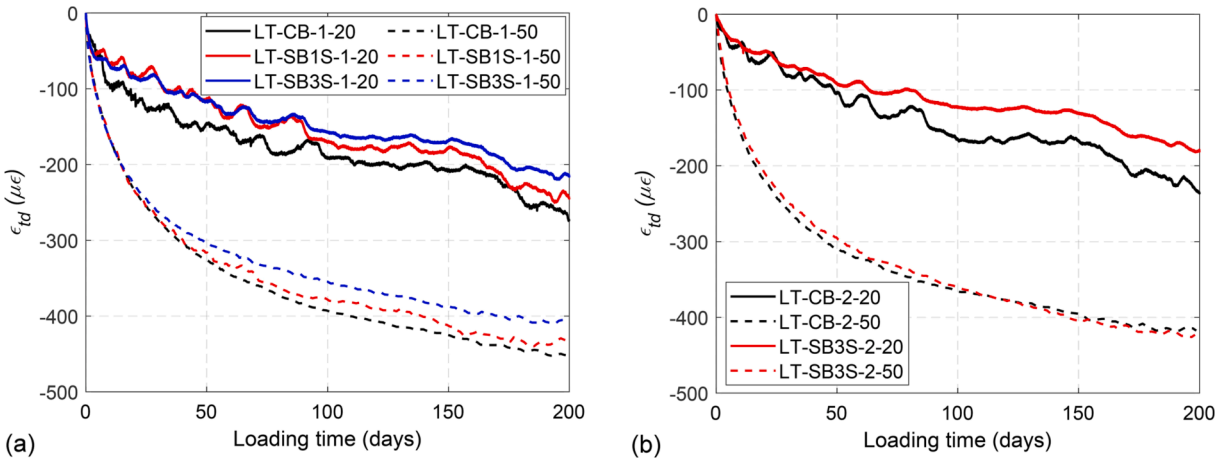

Fig. 14. Top fiber concrete time-dependent strain evolution: (a) Group 1 (ρ = 0.79 %) and (b) Group 2 (ρ = 1.14 %).

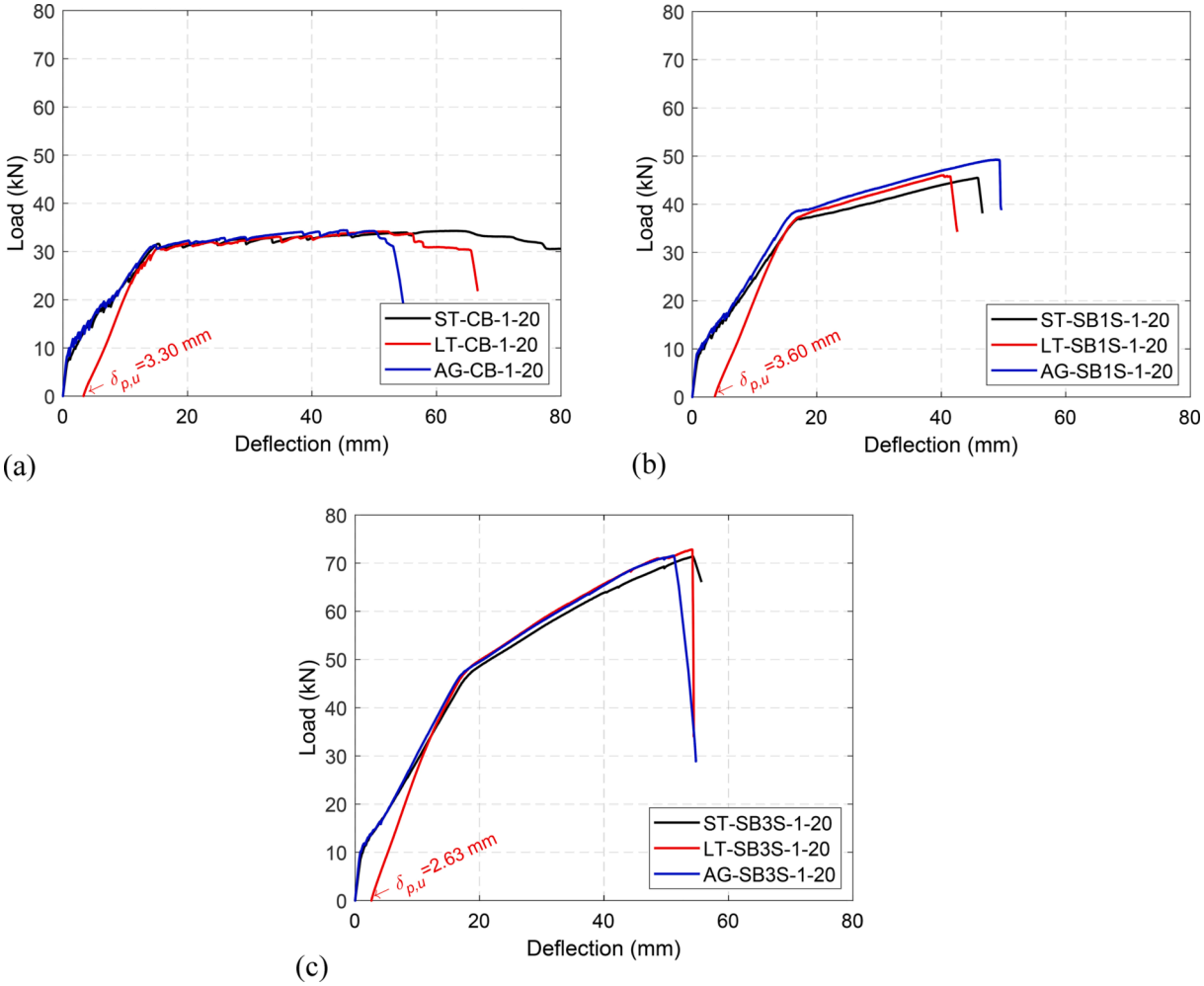

Fig. 15. Representative load–deflection curves for the analysis of residual flexural strength and aging effect: (a) Unstrengthened control beams in Group 1; (b) Strengthened beams with one strip in Group 1; (c) Strengthened beams with three strips in Group 1.

(and curvature), FRP rupture took place (see Fig. 16). This change in failure mode from FRP rupture (FR) to concrete crushing followed by FRP rupture (CC-FR) may be the cause of lower ultimate loads.

The effect of long-term loading is also visible in the initial stiffness of the load–deflection curves. Beams in Series 2 being partially cracked derived in the elastic slope lying between the un-cracked and cracked stages. The stiffness presented in Table 8 was computed as the ratio between load and deflection corresponding to the long-term load level and the service load level. Initial stiffness of specimens subjected to long-term loading (Series 2) were, by far, the largest ones (see Fig. 15 and Table 8). This behavior is similar to what happened during the pre-loading stage, where two cycles of loading/unloading were applied.

Table 8
Results for the analysis of residual flexural strength and aging effect.

Specimen ID	P_y (kN)	P_u (kN)	Stiffness [a] (kN/mm)	$\delta_{p,u}$ (mm)	Failure mode [b]
LT-CB-1–20	30.43	34.17	3.30	3.30	CC
AG-CB-1–20	30.91	34.42	1.41	–	CC
LT-CB-1–50	29.50	34.05	3.06	5.30	CC
LT-SB1S-1–20	37.25	46.03	3.23	3.60	FR
AG-SB1S-1–20	38.68	49.28	1.75	–	FR
LT-SB1S-1–50	35.72	44.90	2.90	4.48	FR
LT-SB3S-1–20	47.00	72.85	3.64	2.63	FR
AG-SB3S-1–20	47.26	71.56	2.12	–	FR
LT-SB3S-1–50	46.48	69.80	3.46	4.01	FR
LT-CB-2–20	38.00	41.07	3.58	2.48	CC
LT-CB-2–50	38.48	42.73	3.47	4.29	CC
LT-SB3S-2–20	53.57	74.41	4.41	2.80	CC-FR
LT-SB3S-2–50	52.46	73.00	4.20	3.38	CC-FR

[a] Computed as the slope of load–deflection curve between long-term load level and service load level.
[b] CC = concrete crushing after steel yielding; FR = FRP rupture; CC-FR = Concrete crushing followed by FRP rupture.

Finally, the effect of high service temperature is reflected in the reduction of initial stiffness, when compared to specimens tested at 20 °C. This is again a consequence of larger concrete time-dependent properties causing larger ultimate permanent deflections after the removal of the long-term load ($\delta_{p,u}$).

For the analysis of the aging effect, results in Series 1 and Series 3 (black and blue lines in Fig. 15, respectively) should be compared. Similar to what was found in the analysis of the residual strength after long-term load, identical load–deflection curves were obtained for unstrengthened control beams and slightly larger yielding loads and post-yielding stiffness were found for strengthened beams. Failure modes of aged beams did not change when compared to that of Series 1.

4. Analytical predictions on time-dependent deflections

In this section, an analytical procedure based on Gilbert [44] is used to predict time-dependent deflections of CFRP NSM strengthened RC elements. Within the procedure, the age-adjusted effective modulus method (AEMM) is used in the cross-sectional analysis to determine how stresses, strains and curvatures vary with time due to creep and shrinkage of concrete. A schematic view of beam cross-section is shown in Fig. 17a. Furthermore, in both types of loading (i.e. short-term and long-term), a linear distribution of strains was assumed (see Fig. 17b).

Assuming a linear strain distribution (as shown in Fig. 17b), the instantaneous response of a cracked section, in terms of instantaneous maximum concrete compressive strain (ε_{0i}) and initial section curvature (κ_i), can be calculated as follows:

$$\varepsilon_{0i} = \frac{BM_{LT} + IN_{LT}}{E_c(AI - B^2)} \tag{3}$$

$$\kappa_i = \frac{AM_{LT} + BN_{LT}}{E_c(AI - B^2)} \tag{4}$$

where M_{LT} and N_{LT} are the moment and axial force applied at the beginning of the long-term loading, respectively ($N_{LT} = 0$ for RC sections under flexural moment only). Moreover, A is the area of the transformed section, and B and I are the first and second moments of inertia of the area of the transformed section, respectively. Furthermore, E_c is the modulus of elasticity of concrete.

Based on Gilbert [44], the variation with time (i.e. time-dependent) of the maximum concrete compressive strain $\Delta\varepsilon_0(t,t_0)$ and section curvature $\Delta\kappa(t,t_0)$ can be calculated as follows:

$$\Delta\varepsilon_0(t,t_0) = \frac{B_e(t,t_0)\Delta M(t,t_0) + I_e(t,t_0)\Delta N(t,t_0)}{E_e(t,t_0)(A_e(t,t_0)I_e(t,t_0) - B_e^2(t,t_0))} \tag{5}$$

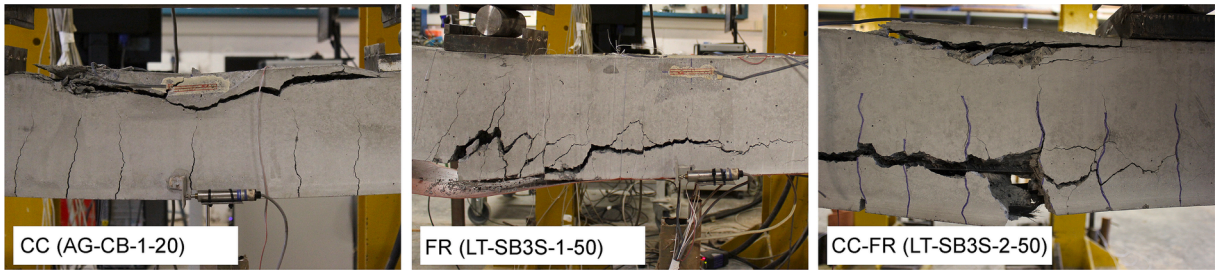

Fig. 16. Representative view of failure modes of the specimens in Series 2 and 3.

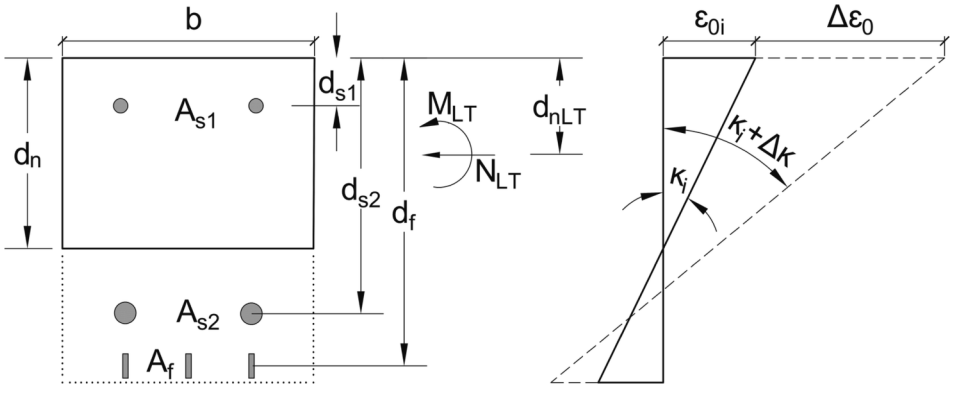

Fig. 17. Time-dependent analysis. (a) Schematic view of beam cross-section and (b) Instantaneous and long-term strains and curvatures in a cracked section.

$$\Delta\kappa(t,t_0)=\frac{A_e(t,t_0)\Delta M(t,t_0)+B_e(t,t_0)\Delta N(t,t_0)}{E_e(t,t_0)(A_e(t,t_0)I_e(t,t_0)-B_e^2(t,t_0))} \quad (6)$$

where t is the age of specimen at the moment considered in days and t_0 is the age of specimen at the beginning of long-term loading in days. In Eqs. (5) and (6), $A_e(t,t_0)$ is the area of the transformed section, and $B_e(t,t_0)$ and $I_e(t,t_0)$ are the first and second moments of inertia of the area of the transformed section, respectively. Finally, $\Delta M(t,t_0)$ and $\Delta N(t,t_0)$ are the restraining force and moment to prevent free development of creep and shrinkage in concrete, and can be calculated as:

$$\Delta N(t,t_0)=E_e(t,t_0)[\varphi_c(t,t_0)(A_c\varepsilon_{oi}-B_c\kappa_i)+\varepsilon_{sh}(t,t_0)A_c] \quad (7)$$

$$\Delta M(t,t_0)=E_e(t,t_0)[\varphi_c(t,t_0)(-B_c\varepsilon_{oi}+I_c\kappa_i)-\varepsilon_{sh}(t,t_0)B_c] \quad (8)$$

where A_c is the area of the concrete section, and B_c and I_c are the first and second moments of inertia of the area of the concrete section (without considering the steel reinforcement), respectively. The instantaneous maximum concrete compressive strain (ε_{0i}) and initial section curvature (κ_i) can be computed from Eqs. (3) and (4), respectively. In addition, $\varphi_c(t,t_0)$ and $\varepsilon_{sh}(t,t_0)$ are the concrete creep coefficient and shrinkage, and $E_e(t,t_0)$ is the effective modulus of elasticity of concrete. In this work, Model Code 2010 [11] predictions for concrete creep coefficient and shrinkage were assumed. Besides, in applying the AEMM, the effective modulus of elasticity of concrete can be obtained as bellow:

$$E_e(t,t_0)=\frac{E_c}{1+\chi(t,t_0)\varphi_c(t,t_0)} \quad (9)$$

where $\chi(t,t_0)$ is the reduction factor for concrete creep coefficient, which can be taken as 0.8 for normal strength concrete [9,12,16,44].

It should be mentioned that, in addition to the explicit mention of $E_e(t,t_0)$ in Eqs. 5–8, the effective modulus of concrete should also be taken into account for the calculation of geometrical properties of the transformed section, by updating the time-dependent steel modular ratio, $n_s(t,t_0)$, and time-dependent FRP modular ratio, n_{FRP} (t,t_0), as follows:

$$n_s(t,t_0)=E_s/E_e(t,t_0) \quad (10)$$

$$n_{FRP}(t,t_0)=E_{FRP}(t,t_0)/E_e(t,t_0) \quad (11)$$

where E_s is the modulus of elasticity of steel reinforcement and $E_{FRP}(t,t_0)$ is the modulus of elasticity of FRP.

4.1. Comparison with experimental results

In this section, analytical predictions following the previously presented methodology are compared to experimental results on time-dependent deflections (shown in Fig. 11). For the analytical predictions, average values for registers on temperature and humidity during the long-term load (see Fig. 4) were used for determining the concrete creep coefficient and shrinkage following Model Code 2010 [11]. In addition, the effect of temperature on mechanical properties of concrete was considered according to Mode Code 2010 [11]. It should be mentioned that temperature gradient in the height of the section causes an additional curvature/deflection that should be taken into account [44]. In this study, due to uniform heating, the difference in temperature between the bottom and top fibers was about 5 °C, thus causing a negligible extra curvature/deflection.

Comparisons of predicted and experimental time-dependent deflections are shown in Figs. 18-20. According to the results, the analytical predictions at 20 °C underestimate the time-dependent deflection, especially for the unstrengthened control beam with lower steel reinforcement ratio (LT-CB-1–20 with ρ = 0.79 %). Focusing on the prediction of the time-dependent deflections in specimens under a high service temperature, in general, analytical predictions overestimate the time-dependent deflection especially for those of the unstrengthened control beams (LT-CB-1–70 and LT-CB-2–70). It is worthy to mention that the presented analytical methodology could be also applied to members subjected to cyclic temperatures, as for instance day-night or summer-winter. In that case, the temperature and humidity histories should be considered as an input in the analytical model.

5. Conclusions

The present experimental work aims to study the long-term performance of NSM CFRP-strengthened RC beams under different service temperatures. An experimental campaign consisting of 23 NSM CFRP-strengthened RC beams was performed, where beams with different steel reinforcement ratios and different amounts of CFRP strengthening area were loaded for 200 days. After that, post long-term tests were carried out to analyze the residual flexural strength as well as the ageing effect. Besides, an analytical procedure for the prediction of time-dependent deflections is presented and compared to experimental results.

As a general conclusion, temperature did not affect the instantaneous flexural performance of NSM CFRP-strengthened RC beams, but had a significant effect on their time-dependent behavior and ultimate permanent deflections. More detailed conclusions are presented next.

From the short-term tests, the following conclusions can be drawn:

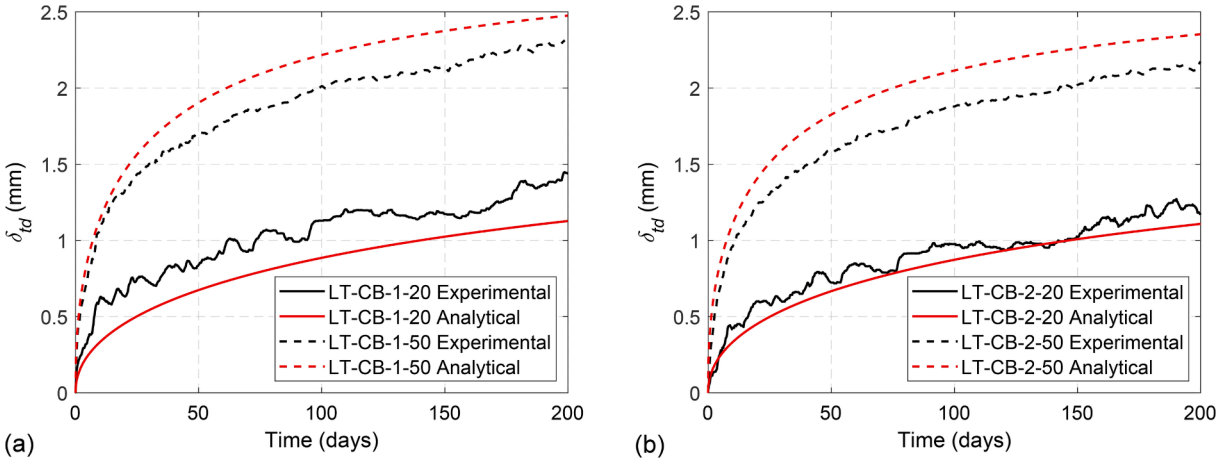

Fig. 18. Analytical predictions and experimental time-dependent deflections for unstrengthened control beams. (a) Group 1 (LT-CB-1–20 and LT-CB-1–50) and (b) Group 2 (LT-CB-2–20 and LT-CB-2–50).

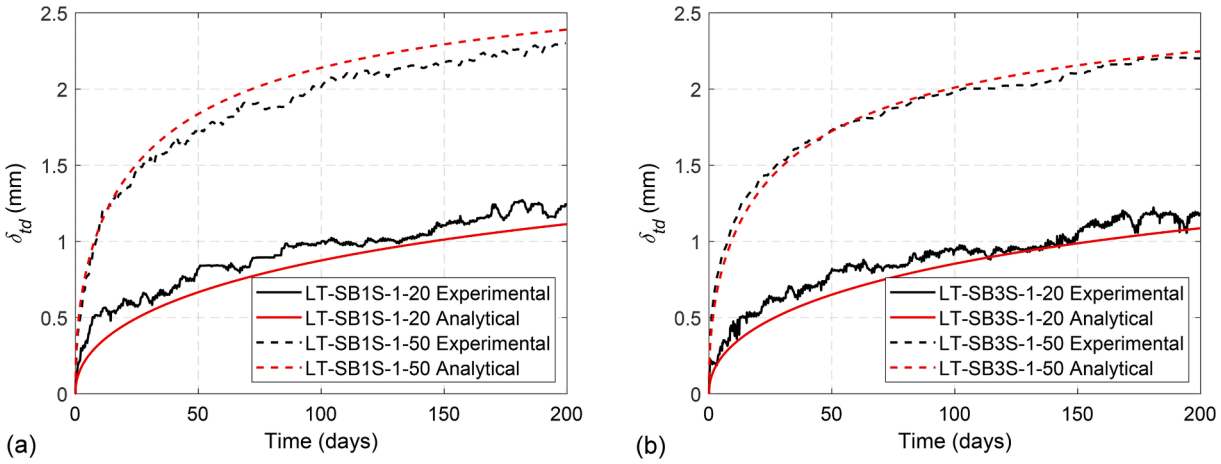

Fig. 19. Analytical predictions and experimental time-dependent deflections for strengthened beams in Group 1 having: (a) one CFRP strip (LT-SB1S-1–20 and LT-SB1S-1–50) and (b) three CFRP strips (LT-SB3S-1–20 and LT-SB3S-1–50).

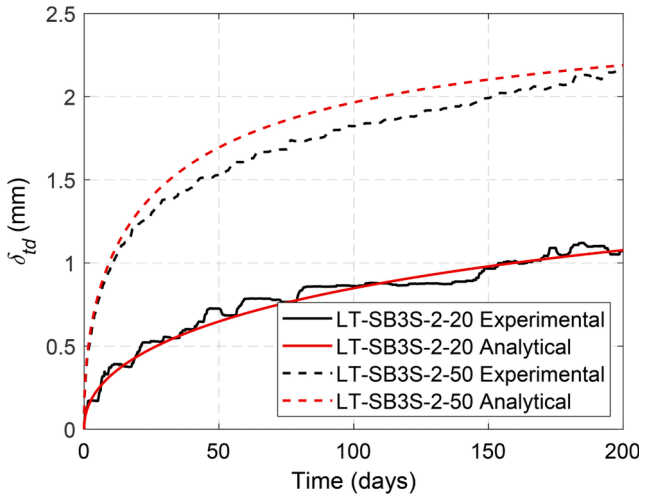

Fig. 20. Analytical predictions and experimental time-dependent deflections for strengthened beams in Group 2 (LT-SB3S-2–20 and LT-SB3S-2–50).

- The increase in the service temperature up to 50 °C had no significant effect on the load–deflection response of the specimens. This can be attributed to this temperature being below the T_g of epoxy adhesive and to an additional possible post-curing of the epoxy adhesive.
- The application of a high service temperature did not affect failure modes, and unstrengthened beams failed by concrete crushing after yielding of the steel reinforcement whilst strengthened beams failed by FRP rupture.

From the long-term tests and analytical predictions, the following conclusions can be drawn:

- The increase in the temperature from 20 °C to 50 °C had an effect on the time-dependent behavior of concrete (larger shrinkage and creep coefficient) and epoxy resin (larger creep coefficient).
- Under 20 °C and the same value of long-term load, lower time-dependent deflections were obtained for beams with larger amounts of FRP strengthening area, as expected. However, for testing temperature equal to 50 °C, the increase in the strengthening area did not have a significant effect on the time-dependent deflections and the time-dependent response of the strengthened beams approached that of the unstrengthened beams.
- The effect of temperature on the time-dependent behavior of concrete appeared to be the dominant factor in time-dependent response of RC beams.
- Analytical predictions based on AEMM and Model Code 2010 were in a good agreement with experimental data.

From the residual flexural strength tests and aging specimens, following conclusions can be drawn:

- Similar to time-dependent deflections, the ultimate permanent deflection of specimens subjected to 50 °C was larger than that of specimens at 20 °C.
- When compared to short-term and aging specimens, no significant change was observed in the residual strength of unstrengthened control beams. On the other hand, for the strengthened beams, a slight increase in yielding load and post-yielding stiffness were found.
- Failure mode of the strengthened specimens with higher reinforcement was changed from FRP rupture to concrete crushing followed by FRP rupture. The rest of the specimens had the same failure mode as in short-term testing.
- The largest initial stiffness was observed for the specimens subjected to long-term load. Furthermore, the specimens subjected to temperature had lower initial stiffness due to larger permanent accumulated deflections.

CRediT authorship contribution statement

Younes Jahani: Conceptualization, Methodology, Validation, Investigation, Data curation, Software, Visualization, Writing – original draft. **Marta Baena:** Conceptualization, Validation, Formal analysis, Writing – review & editing, Supervision, Project administration, Funding acquisition. **Alba Codina:** Validation, Investigation, Writing – review & editing. **Cristina Barris:** Formal analysis, Writing – review & editing, Project administration, Funding acquisition. **Lluís Torres:** Validation, Formal analysis, Writing – review & editing, Supervision.

Declaration of Competing Interest

The authors declare that they have no known competing financial interests or personal relationships that could have appeared to influence the work reported in this paper.

Data availability

Data will be made available on request.

Acknowledgements

This research was supported by the Spanish Ministry of Science and Innovation (MCIN/ AEI) under project PID2020-119015GB-C22 and the Generalitat de Catalunya (under the grant numbers: 2019FI_B 00054 and 2020_FISDU 00476]. The authors also wish to acknowledge the support of S&P Clever Reinforcement Ibérica Lda. for supplying the epoxy resin and the CFRP laminate used in this study.

Data availability

The raw/processed data required to reproduce these findings cannot be shared at this time as the data also forms part of an ongoing study.

References

[1] GangaRao HVS, Taly N, Vijay PV. Reinforced Concrete Design with FRP Composites. CRC Press; 2006.
[2] Nanni A. Fiber-Reinforced-Plastic (FRP) Reinforcement for Concrete Structures: Properties and Application. Amsterdam: Elsevier Science; 1993.
[3] Al-Saadi NTK, Mohammed A, Al-Mahaidi R, Sanjayan J. A state-of-the-art review: Near-surface mounted FRP composites for reinforced concrete structures. Constr Build Mater 2019;209:748–69. https://doi.org/10.1016/j.conbuildmat.2019.03.121.
[4] De Lorenzis L, Teng JG. Near-surface mounted FRP reinforcement: An emerging technique for strengthening structures. Compos Part B 2007;38(2):119–43. https://doi.org/10.1016/j.compositesb.2006.08.003.
[5] Parretti R, Nanni A. Strengthening of RC members using near-surface mounted FRP composites: design overview. Adv Struct Eng 2004;7(6):469–83. https://doi.org/10.1260/1369433042863198.
[6] Pellegrino C, Sena-Cruz J. Design Procedures for the Use of Composites in Strengthening of Reinforced Concrete Structures. State-of-the-Art Report of the Rilem Technical Committee. Springer, The Netherlands, 2016. 10.1007/978-94-017-7336-2.
[7] Daud SA, Forth JP, Nikitas N. Time-dependent behaviour of cracked, partially bonded reinforced concrete beams under repeated and sustained loads. Eng Struct 2018;163:267–80. https://doi.org/10.1016/j.engstruct.2018.02.054.
[8] Mias C, Torres L, Turon A, Sharaky IA. Effect of material properties on long-term deflections of GFRP reinforced concrete beams. Constr Build Mater 2013;41:99–108. https://doi.org/10.1016/j.conbuildmat.2012.11.055.
[9] Kim SH, Han KB, Kim KS, Park SK. Stress–strain and deflection relationships of RC beam bonded with FRPs under sustained load. Compos Part B 2009;40(4):292–304. https://doi.org/10.1016/j.compositesb.2008.12.003.
[10] Malumbela G, Moyo P, Alexander M. Behaviour of RC beams corroded under sustained service loads. Constr Build Mater 2009;23(11):3346–51. https://doi.org/10.1016/j.conbuildmat.2009.06.005.
[11] International Federation for Structural Concrete (fib). Fib Model Code for Concrete Structures 2010. John Wiley & Sons, New York, USA, 2013.
[12] Hong S, Park SK. Long-term behavior of fiber-reinforced-polymer-plated concrete beams under sustained loading: Analytical and experimental study. Compos Struct 2016;152:140–57. https://doi.org/10.1016/j.compstruct.2016.05.031.
[13] Al Chami G, Theriault M, Neale KW. Creep behaviour of CFRP-strengthened reinforced concrete beams. Constr Build Mater 2009;23(4):1640–52. https://doi.org/10.1016/j.conbuildmat.2007.09.006.
[14] Sobuz HR, Ahmed E, Sutan NM, Hasan NMS, Uddin MA, Uddin MJ. Bending and time-dependent responses of RC beams strengthened with bonded carbon fiber composite laminates. Constr Build Mater 2012;29:597–611. https://doi.org/10.1016/j.conbuildmat.2011.11.006.
[15] Li X, Gu X, Ouyang Y, Song X. Long-term behavior of existing low-strength reinforced concrete beams strengthened with carbon fiber composite sheets. Compos Part B 2012;43(3):1637–44. https://doi.org/10.1016/j.compositesb.2012.01.016.
[16] El-Sayed AK, Al-Zaid RA, Al-Negheimish AI, Shuraim AB, Alhozaimy AM. Long-term behavior of wide shallow RC beams strengthened with externally bonded CFRP plates. Constr Build Mater 2014;51:473–83. https://doi.org/10.1016/j.conbuildmat.2013.10.055.
[17] Jiang S, Yao W, Chen J, Tao S. Time dependent behavior of FRP-strengthened RC beams subjected to preload: experimental study and finite element modeling. Compos Struct 2018;200:599–613. https://doi.org/10.1016/j.compstruct.2018.05.110.
[18] Sena-Cruz J, Silva P, Fernandes P, Azenha M, Barros J, Sousa CF, Castro F, Teixeira TAN. Creep behavior of concrete elements strengthened with NSM CFRP laminate strips under different environmental conditions. In: FRPRCS-11: 11th International Symposium on Fiber Reinforced Polymer for Reinforced Concrete Structures. Universidade do Minho, 2013.
[19] Moawad M, Baena M, Barris C, Torres L, Sallam HEM. Time-dependent behavior of NSM strengthened RC beams under sustained loading. Eng Struct 2021;247:113210. https://doi.org/10.1016/j.engstruct.2021.113210.
[20] Kim YJ, Khan F. Creep-induced distress on flexural behavior of reinforced concrete beams retrofitted with near-surface-mounted carbon fiber-reinforced polymer. ACI Struct J 2015;112(4):493–504. https://doi.org/10.14359/51687705.
[21] Kim YJ. Modeling of near-surface-mounted carbon fiber-reinforced polymer for strengthening reinforced concrete beams in sustained load. ACI Struct J 2015;112(6):805–13. https://doi.org/10.14359/51687659.
[22] Emara M, Torres L, Baena M, Barris C, Moawad M. Effect of sustained loading and environmental conditions on the creep behavior of an epoxy adhesive for concrete structures strengthened with CFRP laminates. Compos Part B 2017;129:88–96. https://doi.org/10.1016/j.compositesb.2017.07.026.
[23] Firmo JP, Roquette MG, Correia JR, Azevedo AS. Influence of elevated temperatures on epoxy adhesive used in CFRP strengthening systems for civil engineering applications. Int J Adhes Adhes 2019;93:102333. https://doi.org/10.1016/j.ijadhadh.2019.01.027.
[24] Jahani Y, Baena M, Barris C, Perera R, Torres L. Influence of curing, post-curing and testing temperatures on mechanical properties of a structural adhesive. Constr Build Mater 2022;324:126698. https://doi.org/10.1016/j.conbuildmat.2022.126698.
[25] Silva P, Fernandes P, Sena-Cruz J, Xavier J, Castro F, Soares D, et al. Effects of different environmental conditions on the mechanical characteristics of a structural epoxy. Compos Part B 2016;88:55–63. https://doi.org/10.1016/j.compositesb.2015.10.036.
[26] Barris B, Sala P, Gómez J, Torres L. Flexural behaviour of FRP reinforced concrete beams strengthened with NSM CFRP strips. Compos Struct 2020;241:112059. https://doi.org/10.1016/j.compstruct.2020.112059.
[27] Al-Mahmoud F, Castel A, François R, Tourneur C. RC beams strengthened with NSM CFRP rods and modeling of peeling-off failure. Compos Struct 2010;92(8):1920–30. https://doi.org/10.1016/j.compstruct.2010.01.002.
[28] Al-Mahmoud F, Castel A, François R, Tourneur C. Strengthening of RC members with near-surface mounted CFRP rods. Compos struct 2006;91(2):138–47. https://doi.org/10.1016/j.compstruct.2009.04.040.
[29] Capozucca R. Static and dynamic response of damaged RC beams strengthened with NSM CFRP rods. Compos Struct 2009;91(3):237–48. https://doi.org/10.1016/j.compstruct.2009.05.003.
[30] Reda RM, Sharaky IA, Ghanem M, Seleem MH, Sallam HEM. Flexural behavior of RC beams strengthened by NSM GFRP Bars having different end conditions. Compos Struct 2016;14:131–42. https://doi.org/10.1016/j.compstruct.2016.03.018.
[31] Sena Cruz J, Barros J. Bond between near surface mounted carbon-fiber-reinforced polymer laminate strips and concrete. J Compos Constr 2004;8(6):519–27. https://doi.org/10.1061/(ASCE)1090-0268(2004)8:6(519).
[32] Sena-Cruz J, Barros J, Coelho MR, Silva LF. Efficiency of different techniques in flexural strengthening of RC beams under monotonic and fatigue loading. Constr Build Mater 2012;29:175–82. https://doi.org/10.1016/j.conbuildmat.2011.10.044.
[33] Bilotta A, Ceroni F, Di Ludovico M, Nigro E, Pecce M, Manfredi G. Bond efficiency of EBR and NSM FRP systems for strengthening concrete members. J Compos Constr 2011;15(5):757–72. https://doi.org/10.1061/(ASCE)CC.1943-5614.0000204.
[34] Triantafyllou G, Rousakis T, Karabinis A. Corroded RC beams at service load before and after patch repair and strengthening with NSM CFRP strips. Build 2019;9(3):67. https://doi.org/10.3390/buildings9030067.
[35] Palmieri A, Matthys S, Taerwe L. Fire endurance and residual strength of insulated concrete beams strengthened with near-surface mounted reinforcement. J Compos Constr 2012;17:454–62. http://hdl.handle.net/1854/LU-3238162.
[36] Palmieri A, Matthys S, Taerwe L. Experimental investigation on fire endurance of insulated concrete beams strengthened with near surface mounted FRP bar reinforcement. Compos B Eng 2012;43:885–95. https://doi.org/10.1016/j.compositesb.2011.11.061.
[37] Firmo JP, Correia JR. Fire behaviour of thermally insulated RC beams strengthened with NSM-CFRP strips: experimental study. Compos B Eng 2015;76:112–21. https://doi.org/10.1016/j.compositesb.2015.02.018.
[38] Carlos TB, Rodrigues JPC, de Lima RC, Dhima D. Experimental analysis on flexural behaviour of RC beams strengthened with CFRP laminates and under fire conditions. Compos Struct 2018;189:516–28. https://doi.org/10.1016/j.compstruct.2018.01.094.
[39] Burke PJ, Luke AB, Mark FG. Effects of elevated temperature on near surface mounted and externally bonded FRP strengthening systems for concrete. Cem Concr Compos 2013;35:190–9. https://doi.org/10.1016/j.cemconcomp.2012.10.003.
[40] Jahani Y, Baena M, Gómez J, Barris C, Torres L. Experimental study of the effect of high service temperature on the flexural performance of Near-Surface Mounted (NSM) Carbon Fiber-Reinforced Polymer (CFRP)-Strengthened Concrete Beams. Polymers 2021;13(6):920. https://doi.org/10.3390/polym13060920.
[41] Silva P, Escusa GG, Sena-Cruz J, Azenha M. Experimental investigation of RC slabs strengthened with NSM CFRP system subjected to elevated temperatures up to 80 °C. In: Proc. 8th Int. Conf. on Fibre-Reinforced Polymer (FRP) Composites in Civil Engineering, CICE, Hong Kong, China, 2016. http://hdl.handle.net/1822/43902.
[42] Azevedo AS, Firmo JP, Correia JR, Tiago C. Influence of elevated temperatures on the bond behaviour between concrete and NSM-CFRP strips. Cem Concr Compos 2020;111:103603. https://doi.org/10.1016/j.cemconcomp.2020.103603.

[43] Leone M, Matthys S, Aiello MA. Effect of elevated service temperature on bond between FRP EBR systems and concrete. Compos B Eng 2009;40(1):85–93. https://doi.org/10.1016/j.compositesb.2008.06.004.
[44] Gilbert RI. Time effects in concrete structures. Amsterdam: Elsevier; 1988.
[45] Fib Bulletin 90. Externally Applied FRP Reinforcement for Concrete Structures; International Federation for Structural Concrete: Lausanne, Switzerland, 2019.
[46] UNE-EN 12390-3. Testing Hardened Concrete—Part 3: Compressive Strength of Test Specimens; AENOR: Madrid, Spain, 2003.
[47] UNE-EN 12390-6. Testing Hardened Concrete—Part 6: Tensile Splitting Strength of Test Specimens; AENOR: Madrid, Spain, 2010.
[48] ASTM C469/C469M-14. Standard Test Method for Static Modulus of Elasticity and Poisson's Ratio of Concrete in Compression; ASTM International: West Conshohocken, PA, USA, 2014.
[49] ASTM, ASTM C512 - Standard Test Method for Creep of Concrete in Compression, ASTM International, West Conshohocken, 2010.
[50] UNE-EN ISO 15630-1. Steel for the Reinforcement and Prestressing of Concrete-Test Methods—Part 1: Reinforcing Bars, Wire Rod and Wire; AENOR: Madrid, Spain, 2011.
[51] S&P. S&P Cfrp Laminate, Technical Datasheet; S&P: Seewen, Switzerland, 2017.
[52] ISO 527-5. Plastics-Determination of Tensile Properties—Part 5: Test Conditions FOR Unidirectional Fibre-Reinforced Plastic Composites; ISO: Geneva, Switzerland, 2009.
[53] S&P. S&P Resin 220 HP Epoxy Adhesive, Technical Data Sheet; S&P: Seewen, Switzerland, 2019.
[54] ISO 527-1. Plastics-Determination of Tensile Properties—Part 1: General Principles; ISO: Geneva, Switzerland, 2012.
[55] ASTM E1356-08. Standard Test Method for Assignment of the Glass Transition Temperatures by Differential Scanning Calorimetry; ASTM International: West Conshohocken, PA, USA, 2008.
[56] ASTM D5023-15. Standard Test Method for Plastics: Dynamic Mechanical Properties: In Flexure (Three-Point Bending); ASTM International: West Conshohocken, PA, USA, 2015.
[57] Costa I, Barros J. Tensile creep of a structural epoxy adhesive: experimental and analytical characterization. Int J Adhes Adhes 2015;59:115–24. https://doi.org/10.1016/j.ijadhadh.2015.02.006.
[58] Silva P, Valente T, Azenha M, Sena-Cruz J, Barros J. Viscoelastic response of an epoxy adhesive for construction since its early ages: experiments and modelling. Compos Part B 2016;116:266–77. https://doi.org/10.1016/j.compositesb.2016.10.047.
[59] Majda P, Skrodzewicz JA. Modified creep model of epoxy adhesive at ambient temperature. Int J Adhes Adhes 2009;29(4):396–404. https://doi.org/10.1016/j.ijadhadh.2008.07.010.
[60] Gómez J, Barris C, Jahani Y, Baena M, Torres L. Experimental study and numerical prediction of the bond response of NSM CFRP laminates in RC elements under sustained loading. Constr Build Mater 2021;288:123082. https://doi.org/10.1016/j.conbuildmat.2021.123082.
[61] EN 1992-1-1. Eurocode 2. Design of Concrete Structures—Part 1-1: General Rules and Rules for Buildings; British Standard Institution: London, UK, 2004.